Published in final edited form as:
Arch Biochem Biophys. 2008 January 15; 469(2): 184–194.

Structural and Mechanistic Analysis of Trichodiene Synthase using Site-Directed Mutagenesis: Probing the Catalytic Function of Tyrosine-295 and the Asparagine-225/Serine-229/Glutamate-233–Mg^{2+}_B Motif, [I,II]

L. Sangeetha Vedula[a], **Jiaoyang Jiang**[b], **Tatiana Zakharian**[a], **David E. Cane**[b,*], and **David W. Christianson**[a,*]

a *Roy and Diana Vagelos Laboratories, Department of Chemistry, University of Pennsylvania, Philadelphia, Pennsylvania 19104-6323, USA*

b *Department of Chemistry, Brown University, Providence, Rhode Island 02912-9108, USA*

Abstract

Trichodiene synthase from *Fusarium sporotrichioides* contains two metal ion-binding motifs required for the cyclization of farnesyl diphosphate: the "aspartate-rich" motif **D**^{100}DXX(D/E) that coordinates to Mg^{2+}_A and Mg^{2+}_C, and the "NSE/DTE" motif **N**^{225}DXX**S**XXX**E** that chelates Mg^{2+}_B (boldface indicates metal ion ligands). Here, we report steady-state kinetic parameters, product array analyses, and X-ray crystal structures of trichodiene synthase mutants in which the fungal NSE motif is progressively converted into a plant-like **D**DXX**T**XXX**E** motif, resulting in a degradation in both steady-state kinetic parameters and product specificity. Each catalytically active mutant generates a different distribution of sesquiterpene products, and three newly detected sesquiterpenes are identified. In addition, the kinetic and structural properties of the Y295F mutant of trichodiene synthase were found to be similar to those of the wild-type enzyme, thereby ruling out a proposed role for Y295 in catalysis.

Keywords

enzyme kinetics; protein crystallography; terpenoid cyclase; farnesyl diphosphate

Sesquiterpene synthases catalyze the metal ion-dependent cyclization of the universal acyclic substrate, farnesyl diphosphate (FPP), to form one of more than 300 known monocyclic, bicyclic, or tricyclic hydrocarbon or alcohol products of widely varied structure and stereochemistry [1–5]. These cyclic products represent branch points in terpenoid biosynthesis. Further modifications of cyclic sesquiterpenes and diterpenes involving downstream enzymes such as the cytochrome P450s of *Artemisia annua* and *Taxus brevifolia*, or the Fe(II)-α-

[I]This work was supported by NIH grants GM56838 (D.W.C.) and GM30301 (D.E.C.).

[II]Atomic coordinates and structure factors for N225D trichodiene synthase, the N225D trichodiene synthase-Mg^{2+}_3-PPi complex, N225D/S229T trichodiene synthase, Y295F trichodiene synthase, and the Y295F trichodiene synthase-Mg^{2+}_3-PPi complex have been deposited in the Research Collaboratory for Structural Bioinformatics (http://www.rcsb.org/pdb) with the following accession codes: 2PS4, 2PS5, 2PS6, 2PS7, and 2PS8, respectively.

*Corresponding author. Fax: +1 215-573-2201. *E-mail*: chris@sas.upenn.edu. Fax: +1 401-863-9368. *E-mail*: David_Cane@Brown.edu.

ketoglutarate-dependent hydroxylase PtlH of *Streptomyces avermitilis*, confer highly useful properties on these terpenoid templates by forming products with anticancer, antimalarial, and antibiotic properties [6–8].

The typical FPP cyclization cascade is initiated by the ionization of the allylic diphosphate moiety, triggered by a complex network of hydrogen bond and metal ion coordination interactions. Three catalytically obligatory Mg^{2+} (or Mn^{2+}) ions are required for catalysis [5, 9,10]. These metal ions are coordinated by two conserved signature sequence motifs that characterize all known terpene cyclases: an aspartate-rich motif, which usually appears as **DD**XX(**D,E**); and the so-called NSE/DTE motif, which usually appears as (**N,D**)DXX(**S**,**T**)XXX(**E,D**) (boldface type indicates typical metal ion ligands). Comparison of 54 plant, fungal, and microbial cyclases reveals that the second metal ion-binding motif is conserved as **N**DXX**S**XXX**E** in most fungal and microbial enzymes, while it occurs as **D**DXX**T**XXX**E** in most plant cyclases [11, current studies].

Trichodiene synthase from *Fusarium sporotrichioides* is an 89 kDa homodimer that catalyzes the cyclization of FPP to form trichodiene as the major product [10,13] (Fig. 1). This cyclase contains the aspartate-rich motif D^{100}DSKD (D100 coordinates to $Mg^{2+}{}_A$ and $Mg^{2+}{}_C$; D^{104} does not coordinate to metal ions in this cyclase) and the NSE/DTE motif $N^{225}S^{229}E^{233}$ (these residues chelate $Mg^{2+}{}_B$) [14]. Site-directed mutagenesis of the aspartate-rich motif has established that substitution of glutamate for D100 or D101 decreases the catalytic efficiency (k_{cat}/K_M) of the enzyme 22-fold or 6-fold, respectively, in comparison with the wild-type enzyme, and decreases the proportion of trichodiene formed with a concomitant increase in the generation of several additional sesquiterpene coproducts [15]. X-ray crystal structures of D100E trichodiene synthase and its complex with $Mg^{2+}{}_3$-PP_i reveal that the diphosphate-triggered active site closure observed in the wild-type enzyme [14] is highly attenuated in this mutant, perhaps as a consequence of incomplete metal ion binding ($Mg^{2+}{}_C$ is not observed) [16]. Compromised metal ion binding is thus associated with a decrease in both the rate and the specificity of catalysis.

To date, the dissection of the NSE/DTE-$Mg^{2+}{}_B$ coordination motif in terpene cyclases by site-directed mutagenesis has not been accompanied by X-ray crystal structure analysis. Accordingly, we now report the first exploration of structure-function relationships for this motif in trichodiene synthase. In particular, we probe the apparent preference for NSE in microbial and fungal cyclases and DTE in plant cyclases. We also report the structure and function of the Y295F mutant to test a proposed role for this residue as a general base during catalysis [16]. Surprisingly, although the wild-type and mutant enzymes generate predominantly trichodiene, all active enzymes are found to generate up to 16 different sesquiterpene products, based on gas chromatographic and mass spectrometric (GC/MS) analysis of product mixtures.

Materials and Methods

Site-directed mutagenesis

Single site-specific mutations were introduced in the wild-type expression vector pZW03, using Stratagene's QuikChange Site-Directed Mutagenesis kit. Optimal PCR conditions were previously described [17]. The plasmid for the N225D/S229T double mutant was generated by using the N225D plasmid as template.

Expression, purification, and crystal structure determination of trichodiene synthase mutants

The plasmid containing the gene encoding each trichodiene synthase variant was transformed into *Escherichia coli* BL21 (DE3), overexpressed, purified, and crystallized by the hanging drop vapor diffusion method as described for wild-type trichodiene synthase [14]. The complexes between mutant trichodiene synthases and pyrophosphate (PP_i) were prepared using the same crystal soaking protocol used for the preparation of the complex with wild-type trichodiene synthase [14]. The mutant trichodiene synthases crystallized essentially isomorphously with the wild-type enzyme (space group $P3_121$, $a = b = 122.2$ Å, $c = 151.2$ Å) [14]. We were unable to grow crystals of S229T trichodiene synthase. Crystals were prepared for data collection by cryoprotection in 25% ethylene glycol and flash cooling in liquid nitrogen.

Diffraction data were collected at the Advanced Light Source, Berkeley (beamline 5.0.2), National Synchrotron Light Source, Brookhaven National Laboratory (beamline X12C) and Cornell High Energy Synchroton Source (beamline F1). Data were indexed and merged using the program MOSFLM/Scala [18,19] or HKL2000 [20]. The structures were solved by the difference Fourier technique. The programs CNS [21] and O [22] were used in refinement and rebuilding, respectively. Noncrystallographic symmetry constraints were used in the initial stages of refinement and subsequently relaxed into appropriately weighted restraints as judged by R_{free} as refinement progressed. Molecular models shown in the figures were prepared with Bobscript version 2.4 or Raster3D version 2.7d [23–25]. Data collection and refinement statistics are reported in Table 1.

Determination of kinetic parameters of mutant trichodiene synthases

Trichodiene synthase mutants were assayed as previously described [26] in 10 mM Tris (pH 7.8), 5 mM $MgCl_2$, 15 % glycerol, and 5 mM β-mercaptoethanol. Each series of assays was performed 2–4 times using concentrations of [1-^{3}H]FPP (80–100 mCi/mmol) ranging from 0.025–60 μM. Optimal enzyme concentration was determined by incubating a fixed amount of radiolabeled substrate with varying concentrations of each mutant enzyme. A concentration at which the enzyme concentration dependence of product formation was linear, and where <10 % of substrate was turned over, was used for determination of kinetic parameters. The mixture was overlaid with 0.75 mL of hexane immediately after addition of enzyme and incubated for 7–10 min at 27–30 °C. The reaction was quenched by addition of 75 μL of 100 mM EDTA (pH 8.0) and vortexed for 25 s. The mixture was vortexed with an additional 0.75 mL of hexane before extraction of products. Hexane was removed using a Pasteur pipette. The hexane extract was passed through a silica gel column directly into a scintillation vial containing 5 mL of scintillation fluid. The aqueous phase was extracted with an additional 2 X 0.75 mL of hexane and passed through the same silica gel column. Finally, the column was washed with an additional 0.75 mL hexane. The scintillation counts were measured using a Beckman scintillation counter.

Alternatively, the reaction mixture was overlaid with 1 mL ethyl acetate in a screw-cap glass vial immediately after addition of enzyme and the cap was tightly screwed on before incubation at 30 °C. After 7–10 min, the reaction mixture was vortexed for 30 s. Ethyl acetate denatures the enzyme to quench the reaction. After the organic and aqueous layers separated, 0.4 mL of ethyl acetate was removed and added to scintillation fluid. For each substrate concentration, a blank was run to account for buffer-catalyzed FPP solvolysis. The counts for each blank were subtracted from the corresponding counts for the reaction mixture and corrected for the total volume.

Incubation of mutant trichodiene synthases with farnesyl diphosphate

Analysis of cyclization products generated from FPP was performed using gas chromatography–mass spectroscopy (GC/MS) as previously described [13,15]. All glassware was washed and baked in an oven prior to use to ensure the removal of any possible trace contaminants. Farnesyl diphosphate (50–500 μM) was incubated with or without purified wild-type or mutant trichodiene synthase (1 mg) in 4 mL buffer (10 mM Tris (pH 7.8), 5 mM $MgCl_2$, 15% glycerol, and 5 mM β-mercaptoethanol) and overlaid with HPLC-grade *n*-pentane (Fisher P399-1) in a glass test tube at 30 °C for 3–20 h. Reaction products were extracted with HPLC-grade *n*-pentane and the extracts were purified on a 3-cm 230–400 mesh silica gel column. The purified extract was concentrated on an ice-water mixture under reduced pressure until the volume decreased to <50 μL and the concentrate was analyzed by GC/MS. Reaction products were initially analyzed using a Hewlett–Packard 6890 gas chromatograph (GC) coupled to a 5973 mass selective detector (MSD) operating in a CI mode, and equipped with an HP-5MS capillary column (0.25 mm i.d. x 30 m with 0.25μm film) (Agilent Technologies). 2 μL of analyte was injected in splitless mode into the gas chromatograph-mass spectrometer. The oven temperature was maintained at 35 °C for 1 min, increased at the rate of 5 °C/min to 230 °C, followed by a 20 °C/min increase to 280 °C. The temperature was held at 280 °C for 20 min.

Identification of products generated by D100E trichodiene synthase

GC/MS (electron ionization or EI) was performed on a Hewlett-Packard Series 2 GC-MSD and equipped with an HP-5MS capillary column (30 m x 0.25 mm) at 70 eV EI, operating in a positive ion mode. The oven temperature was increased from 50 °C to 280 °C, at a rate of 5 °C/min. Each of the products was identified by direct comparison with the spectra of the corresponding reference compounds in the MassFinder 3.0 Library (http://massfinder.com) or with those of authentic standards.

Results

Kinetic parameters of trichodiene synthase mutants

Interestingly, relatively conservative amino acid substitutions in the NSE/DTE motif result in significant changes in catalytic efficiency. The N225D mutation results in only a 6-fold increase in K_M, but with k_{cat} decreased by 28-fold, the overall catalytic efficiency (k_{cat}/K_M) is diminished 177-fold relative to that of the wild-type enzyme (Table 2). The S229T mutation results in a 77-fold increase in K_M, but with k_{cat} decreased by only 9-fold the overall catalytic efficiency is diminished 708-fold (Table 2). Notably, S229T trichodiene synthase has a short half-life and 90 nM protein samples become inactive in less than a day. The N225D/S229T mutant is completely inactive under the conditions of the assay. Finally, the kinetic parameters for Y295F trichodiene synthase (Table 2) are not significantly different from those observed for the wild-type enzyme [26].

Product array analysis of wild-type and mutant trichodiene synthases

Incubation of wild-type and mutant trichodiene synthases with FPP generates trichodiene as the major product along with up to 15 additional products [13, current studies]. Five of the additional products were identified in previous studies of D100E trichodiene synthase: β-farnesene, α-bisabolene, β-bisabolene, cuprenene, and isochamigrene [15]. Three more of the additional products were identified as α-barbatene, α-acoradiene, and β-acoradiene; proposed cyclization mechanisms are shown in Fig. 1. These sesquiterpene products were identified by comparison with authentic standards or by comparison of retention index ± 5) and EI-mass spectrum with terpenes in the MassFinder 3.0 Terpenoids Library of Dr. Detlev H. Hochmuth (http://www.massfinder.com). The remaining seven minor products could not be identified,

however, due to low concentrations or absence of matching compounds in the MassFinder and other MS data libraries. Product arrays of known products of wild-type and mutant trichodiene synthases are summarized in Table 3 and both EI and CI mass spectra of identified products can be found in the Supplementary Material.

N225D trichodiene synthase structures

The crystal structure of unliganded N225D trichodiene synthase is identical to that of the wild-type enzyme [14] with only minor differences evident in side chain conformations (Fig. 2). The r.m.s. deviation for 349 C_α atoms between the two structures is 0.55 Å. Interestingly, as also observed in unliganded R304K trichodiene synthase [17], unliganded N225D trichodiene synthase binds one Mg^{2+} ion coordinated by D100 and E164 in the active site of monomer B (Fig. 2a). This metal ion most closely corresponds to $Mg^{2+}{}_C$ in the structure of the wild-type enzyme complexed with $Mg^{2+}{}_3$-PP_i [14].

In the N225D trichodiene synthase-$Mg^{2+}{}_3$-PP_i complex, the $Mg^{2+}{}_3$-PP_i cluster binds to the active site of monomer B of the dimer (Fig. 3). This monomer undergoes diphosphate-induced conformational changes, with D101 and R304 forming a salt link to cap the active site cavity, as observed for the PP_i-bound wild-type enzyme [14]. The r.m.s. deviation between the unliganded and liganded forms of this mutant is 1.4 Å for 349 C_α atoms, and the r.m.s. deviation between the $Mg^{2+}{}_3$-PP_i complexes of the mutant and wild-type enzymes is 0.19 Å for 349 C_α atoms. These r.m.s. deviations indicate that N225D trichodiene synthase undergoes complete active site closure upon the binding of $Mg^{2+}{}_3$-PP_i. Notably, the $Mg^{2+}{}_B$ coordination polyhedron is essentially identical to that observed in the wild-type enzyme, with D225 occupying the coordination site formerly occupied by N225 (Fig. 3). As a consequence of the N225D substitution, however, the $Mg^{2+}{}_B$-O coordination distance for residue 225 shortens from 2.5 Å to 2.3 Å, and the $Mg^{2+}{}_B$-O coordination distance for E233 (which is opposite residue 225) lengthens from 2.0 Å to 2.6 Å due in part to a 36° conformational change in sidechain torsion angle χ_3. These structural changes may be due to the additional negative charge introduced by the N225D substitution in the $Mg^{2+}{}_B$ coordination polyhedron. Additionally, $Mg^{2+}{}_C$ and $Mg^{2+}{}_A$ move by 0.4 Å and 0.3 Å relative to their positions in the PP_i-bound wild-type enzyme [14], even though these metal ions do not interact directly with D225.

N225D/S229T trichodiene synthase structure

The structure of this mutant is generally similar to that of the wild-type enzyme, but some differences are observed for the conformations of certain active site residues, e.g., E233 and R304 (Fig. 4) [14]. The r.m.s. deviation of 349 C_α atoms with the wild-type enzyme is 0.87 Å. The double mutation may affect binding of co-product PP_i, since we were unable to prepare crystals of the complex with $Mg^{2+}{}_3$-PP_i.

Y295F trichodiene synthase structures

The structure of this mutant is generally similar to that of wild-type trichodiene synthase (Fig. 5) [14]. Although the r.m.s. deviation with the wild-type enzyme of 349 C_α atoms of 0.94 Å is relatively high in comparison with r.m.s. deviations of other mutant trichodiene synthase structures determined to-date [14,16,17], this is largely due to differences in some poorly ordered segments in the mutant, e.g., the *N*-terminal P5-T28 segment and the L307-Y329 loop. Regardless, it is clear that the Y295F substitution does not introduce significant structural perturbations in the active site.

Interestingly, as with R304K [17] and N225D trichodiene synthases, unliganded Y295F trichodiene synthase binds one Mg^{2+} ion in the active site of monomer B (Fig. 5a). This metal ion is coordinated by D100 and E164, as observed in R304K and N225D trichodiene synthases,

and it most closely corresponds to Mg^{2+}_C in the structure of the wild-type enzyme complexed with Mg^{2+}_3-PP_i [14].

Finally, the structure of Y295F trichodiene synthase complexed with Mg^{2+}_3-PP_i is identical to that of the Mg^{2+}_3-PP_i complex with the wild-type enzyme (Fig. 6) [14], with an r.m.s. deviation of 0.23 Å for 349 C_α atoms. The metal ion-binding site appears to be slightly perturbed, however, such that the r.m.s. deviation of the metal ion positions in this mutant complex with that of the wild-type enzyme complex is 0.6 Å. The binding of the Mg^{2+}_3-PP_i cluster results in complete active site closure, with an r.m.s. deviation of 0.99 Å for 349 C_α atoms in comparison with the uncomplexed mutant enzyme.

Discussion

Catalytic importance of the NSE/DTE motif

Substrate affinity is not substantially attenuated in N225D trichodiene synthase, as indicated by only a 4-fold increase in K_M (Table 2). Moreover, since the structure of the Mg^{2+}_3-PP_i complex is essentially identical for the N225D mutant and the wild-type enzyme, it is reasonable to expect that the binding of the Mg^{2+}_3-FPP complex is also identical in the mutant and wild-type enzymes. The apparently slight attenuation of substrate affinity may result from the introduction of an additional negative charge from the protein to the Mg^{2+}_B coordination polyhedron, which in turn would weaken the charge-charge interaction between Mg^{2+}_B and FPP. The 28-fold reduction in k_{cat} may similarly result from Mg^{2+}_B coordination phenomena, for example if the additional negative charge in the metal ion coordination polyhedra compromises the metal ion-dependent activation of the diphosphate leaving group in the first step of catalysis, or if it compromises the release of Mg^{2+}_B that may accompany rate-determining product dissociation [27].

A more significant effect on catalysis is observed for S229 mutants of trichodiene synthase. The 77-fold increase in K_M measured for S229T trichodiene synthase is the highest observed thus far for a trichodiene synthase mutant. This may be a consequence of the energetic cost for the conformational change of this side chain between the metal ion-free and metal ion-bound structures. In the wild-type enzyme, S229 undergoes a 142° rotation around side chain torsion angle χ_1 in order to achieve Mg^{2+}_B coordination. Analysis of the wild-type enzyme structure [14] suggests that the nearby side chain of Y305 (which donates a hydrogen bond to PP_i in the wild-type enzyme) may sterically hinder this conformational change in S229T trichodiene synthase. Additionally, the Cγ atom of the T229 side chain would clash with the main chain atoms of residues D225 or D226, or the side chain of E233. Thus, the S229T substitution may perturb this region of the protein structure. In bornyl diphosphate synthase, the corresponding residue, T500, does not undergo a conformational change upon the binding of ligands [28].

In comparison, residue Y305 of trichodiene synthase corresponds to Y572 of bornyl diphosphate synthase, a plant monoterpene cyclase. However, Y572 does not interact with the diphosphate moiety or with T500 in the DTE motif of bornyl diphosphate synthase [28], so the specific intramolecular and intermolecular interactions of residues in the NSE/DTE motif and their neighbors appear to have divergently evolved in fungal and plant cyclases based on these two examples. Accordingly, it is not straightforward to swap the NSE-Mg^{2+}_B motif of a microbial or fungal cyclase with the DTE-Mg^{2+}_B motif of a plant cyclase. The complete inactivity of N225D/S229T trichodiene synthase (Table 2) is probably due to a combination of the additional negative charge in the Mg^{2+}_B coordination polyhedron as well as the hindered conformational changes required for the bulkier T229 residue to achieve Mg^{2+}_B coordination.

Catalytic importance of Y295

Previous modeling studies of carbocation intermediates in the trichodiene synthase active site had suggested that Y295 could conceivably serve as the catalytic base responsible for the deprotonation of the final carbocation intermediate (Fig. 1) [16]. GC/MS analysis of the reaction products from both wild-type and Y295F trichodiene synthases reveals, however, that the major product of each enzyme is trichodiene (Table 3). Moreover, since Y295F trichodiene synthase exhibits nearly identical kinetic parameters to those of the wild-type enzyme (Table 2), we conclude that Y295 does *not* function as a general base in the trichodiene synthase mechanism.

If Y295 is not the general base that catalyzes the final proton abstraction in the trichodiene synthase mechanism, then what alternatives remain? Structural studies of farnesyl diphosphate synthase and aristolochene synthase indicate that the distal oxygen of the substrate diphosphate moiety is ideally positioned to abstract a proton from the final carbocation intermediate [29, 30]. Moreover, structural studies of wild-type and Y305F trichodiene synthases complexed with Mg^{2+}_3-PP_i reveal a water molecule trapped in the active site that coordinates to Mg^{2+}_C [14,31], and structural studies of bornyl diphosphate synthase reveal a water molecule trapped in the active site along with the cyclization product [28]. Therefore, we speculate that either the PP_i anion or a trapped water molecule serves as the final general base in the trichodiene synthase mechanism.

Mechanistic inferences regarding product diversity

The hydrophobic and aromatic residues lining the active site cleft of trichodiene synthase form a template that enforces the proper conformation and orientation of the flexible FPP substrate and subsequently formed carbocation intermediates leading to formation of trichodiene. This template, however, is somewhat permissive in the wild-type enzyme as indicated by the observation of low percentages of alternative cyclization products [13] (Table 3). Significantly, this permissiveness is exaggerated in most active site mutants, and it is suggested that the structural basis of such product promiscuity is simply the increased volume of the active site cleft [16,31]. It is also notable that a single-point mutation can cause a preferential increase in the generation of one particular alternative product. For example, the Y295F mutation causes a 19-fold increase in the generation of β-bisabolene relative to the fraction of this sesquiterpene side product generated by the wild-type enzyme (Table 3). The Y295F mutant exhibits an active site contour and kinetic parameters that are generally similar to those of the wild-type enzyme [14], so it is clear that even subtle changes to the active site template for FPP cyclization – the substitution of a hydrogen atom for a hydroxyl group – can result in significantly altered product arrays. This phenomenon is reminiscent of Keasling's results with γ-humulene synthase mutants, in which 3–5 simultaneous mutations in the active site template alter and refocus product selectivity without compromising overall activity [32]. It is possible that multiple mutations in the active site template of trichodiene synthase may similarly lead to the formation of new sesquiterpene products. The alteration of residues that buttress the active site can also dramatically refocus the cyclization specificity of a sesquiterpene cyclase [33], demonstrating that subtle changes in the active site contour caused by mutation of neighboring residues rather than residues defining the cleft itself can result in altered product arrays.

Strikingly, the observation of the two acoradiene diastereomers in the product arrays of both wild type and mutant trichodiene synthases provides the first evidence that trichodiene synthase is capable of generating and stabilizing both (*R*)- and (*S*)-bisabolyl cations in its active site: the (*R*)-bisabolyl carbocation is an intermediate in trichodiene biosynthesis, and the (*S*)-bisabolyl carbocation is an intermediate in acoradiene biosynthesis (Fig. 1).

Similarly striking is the identification of α-barbatene in the product array of wild-type and mutant trichodiene synthases (Table 3), the biosynthesis of which must proceed through several new intermediates derived from the (*R*)-bisabolyl cation (Fig. 1). This is the first tricyclic sesquiterpene product identified for trichodiene synthase and its generation clearly requires a permissive active site template to accommodate the steric demands of the third cyclization reaction illustrated in Fig. 1. Future mutagenesis and structural studies of trichodiene synthase will allow us to probe and define the structural basis of specificity in the formation of alternative cyclization products.

Supplementary Material

Refer to Web version on PubMed Central for supplementary material.

Acknowledgements

We thank the Advanced Light Source at Lawrence Berkeley National Laboratory, National Synchrotron Light Source at Brookhaven National Laboratory, and Cornell High Energy Synchrotron Source for access to X-ray crystallographic data collection facilities, and we thank Dr. Barry Cooperman for access to his laboratory scintillation counter.

Abbreviations

FPP
: farnesyl diphosphate

PP_i
: inorganic pyrophosphate

r.m.s.
: root mean square

CI
: chemical ionization

EI
: electron ionization

GC
: gas chromatography

MS
: mass spectrometry

MSD
: mass selective detector

References

1. Cane DE. Acc Chem Res 1985;18:220–226.
2. Croteau, R.; Cane, DE. Methods in Enzymology. Steroids and Isoprenoids (Part A). 110. Academic Press; New York: 1985. p. 383-405.
3. Cane DE. Chem Rev 1990;90:1089–1103.
4. Wendt KU, Schulz GE. Structure 1998;6:127–133. [PubMed: 9519404]
5. Christianson DW. Chem Rev 2006;106:3412–3442. [PubMed: 16895335]
6. Teoh KH, Polichuk DR, Reed DW, Nowak G, Covello PS. FEBS Lett 2006;580:1411–1416. [PubMed: 16458889]
7. Kaspera R, Croteau R. Phytochem Rev 2006;5:433–444.

8. You Z, Omura S, Ikeda H, Cane DE. J Am Chem Soc 2006;128:6566–6567. [PubMed: 16704250]
9. Hohn TM, Plattner RD. Arch Biochem Biophys 1989;272:137–143. [PubMed: 2544140]
10. Hohn TM, VanMiddlesworth F. Arch Biochem Biophys 1986;251:756–761. [PubMed: 3800398]
11. Cane DE, Kang I. Arch Biochem Biophys 2000;376:354–364. [PubMed: 10775423]
12. Cane DE, Swanson S, Murthy PPN. J Am Chem Soc 1981;103:2136–2138.
13. Vedula LS, Zhao Y, Coates RM, Koyama T, Cane DE, Christianson DW. Arch Biochem Biophys 2007;466:260–266. [PubMed: 17678871]
14. Rynkiewicz MJ, Cane DE, Christianson DW. Proc Natl Acad Sci USA 2001;98:13543–13548. [PubMed: 11698643]
15. Cane DE, Xue Q, Fitzsimons BC. Biochemistry 1996;35:12369–12376. [PubMed: 8823172]
16. Rynkiewicz MJ, Cane DE, Christianson DW. Biochemistry 2002;41:1732–1741. [PubMed: 11827517]
17. Vedula LS, Cane DE, Christianson DW. Biochemistry 2005;44:12719–12727. [PubMed: 16171386]
18. Leslie AGW. Joint CCP4 + ESF-EAMCB Newsletter on Protein Crystallography 1992;26
19. Collaborative Computational Project, Number 4. Acta Crystallogr 1994;D50:760–763.
20. Otwinowski, Z.; Minor, W. Methods in Enzymology. Macromolecular Crystallography (Part A). 276. Academic Press; San Diego: 1997. p. 307-326.
21. Brünger AT, Adams PD, Clore GM, DeLano WL, Gros P, Grosse-Kunstleve RW, Jiang JS, Kuszewski J, Nilges M, Pannu NS, Read RJ, Rice LM, Simonson T, Warren GL. Acta Crystallogr 1998;D54:905–921.
22. Jones TA, Zou JY, Cowan SW, Kjeldgaard M. Acta Crystallogr 1991;A47:110–119.
23. Bacon DJ, Anderson WF. J Molec Graphics 1988;6:219–220.
24. Merritt EA, Murphy MEP. Acta Crystallogr 1994;D50:869–873.
25. Merritt, EA.; Bacon, DJ. Methods in Enzymology. Macromolecular Crystallography (Part B). 277. Academic Press; San Diego: 1997. p. 505-524.
26. Cane DE, Yang G, Xue Q, Shim JH. Biochemistry 1995;34:2471–2479. [PubMed: 7873526]
27. Cane DE, Chiu HT, Liang PH, Anderson KS. Biochemistry 1997;36:8332–8339. [PubMed: 9204880]
28. Whittington DA, Wise ML, Urbansky M, Coates RM, Croteau RB, Christianson DW. Proc Natl Acad Sci USA 2002;99:15375–15380. [PubMed: 12432096]
29. Hosfield DJ, Zhang Y, Dougan DR, Broun A, Tari LW, Swanson RV, Finn J. J Biol Chem 2004;279:8526–8529. [PubMed: 14672944]
30. Shishova EY, Di Costanzo L, Cane DE, Christianson DW. Biochemistry 2007;46:1941–1951. [PubMed: 17261032]
31. Vedula LS, Rynkiewicz MJ, Pyun HJ, Coates RM, Cane DE, Christianson DW. Biochemistry 2005;44:6153–6163. [PubMed: 15835903]
32. Yoshikuni Y, Ferrin TE, Keasling JD. Nature 2006;440:1078–1082. [PubMed: 16495946]
33. Greenhagen BT, O'Maille PE, Noel JP, Chappell J. Proc Natl Acad Sci USA 2006;103:9826–9831. [PubMed: 16785438]
34. Hong YJ, Tantillo DJ. Org Lett 2006;8:4601–4604. [PubMed: 16986960]

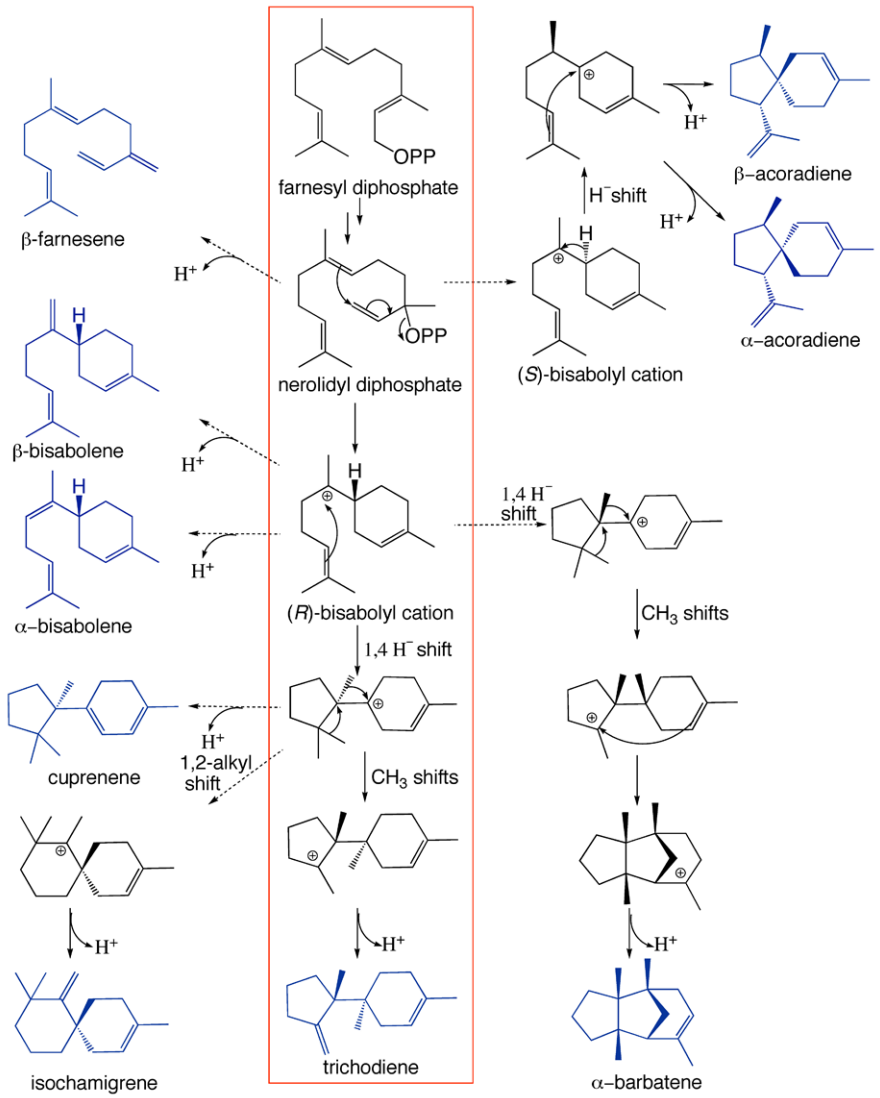

Fig. 1.

Red box: Postulated mechanism for the cyclization of farnesyl diphosphate (FPP) to trichodiene by trichodiene synthase; OPP = diphosphate, NPP = nerolidyl diphosphate [12]. For a proposed mechanistic variation, see the recently reported work of Hong and Tantillo [34]. Proposed mechanisms leading to alternative sesquiterpene products are also indicated.

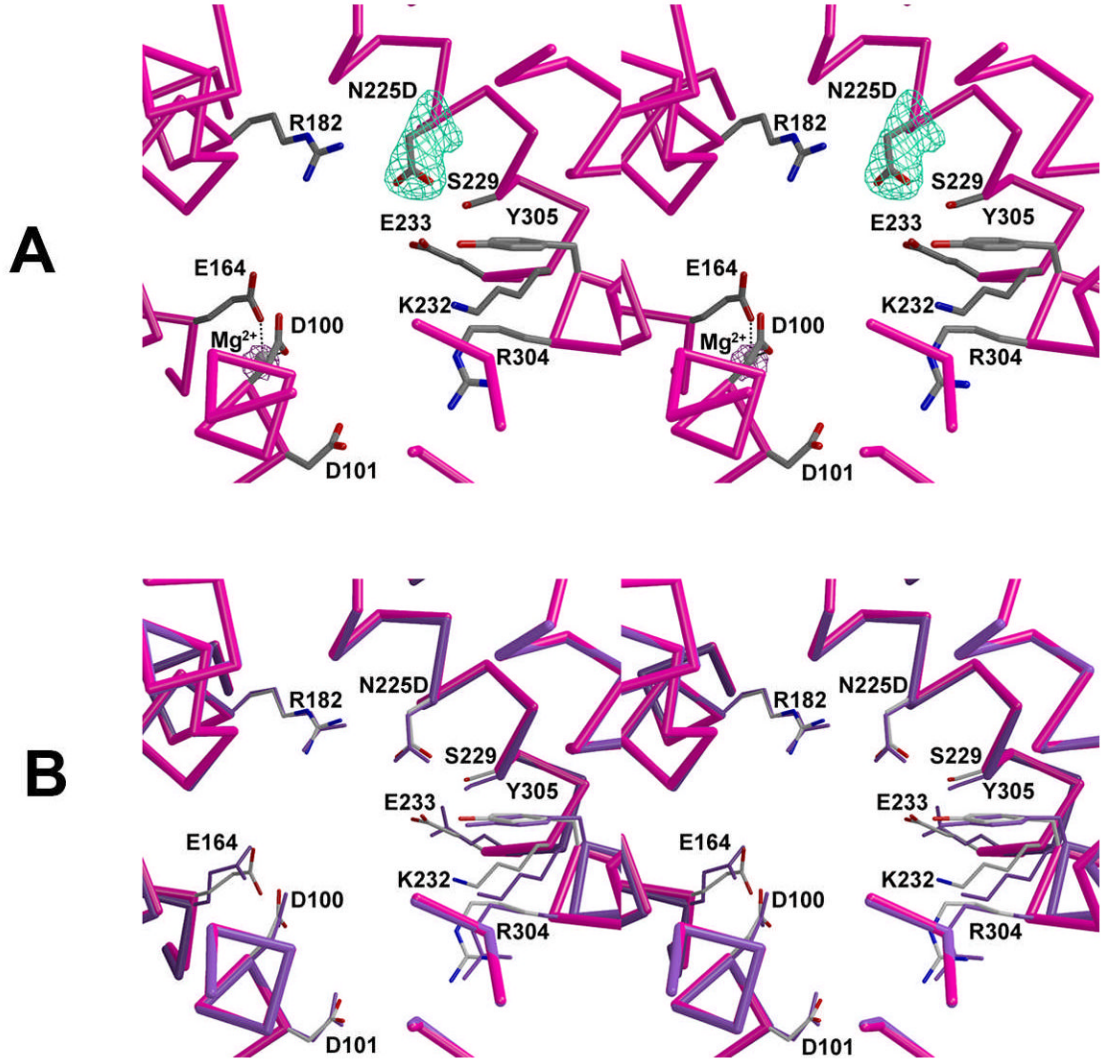

Fig. 2.

Active site of unliganded N225D trichodiene synthase. **(a)** Simulated annealing omit maps of D225 and magnesium ion are shown in cyan (4.7Å) and maroon (6.0Å), respectively. The Mg^{2+} ion is shown as a gray sphere. Metal ion coordination interactions are shown in black. **(b)** Superposition with the active site of unliganded trichodiene synthase (purple).

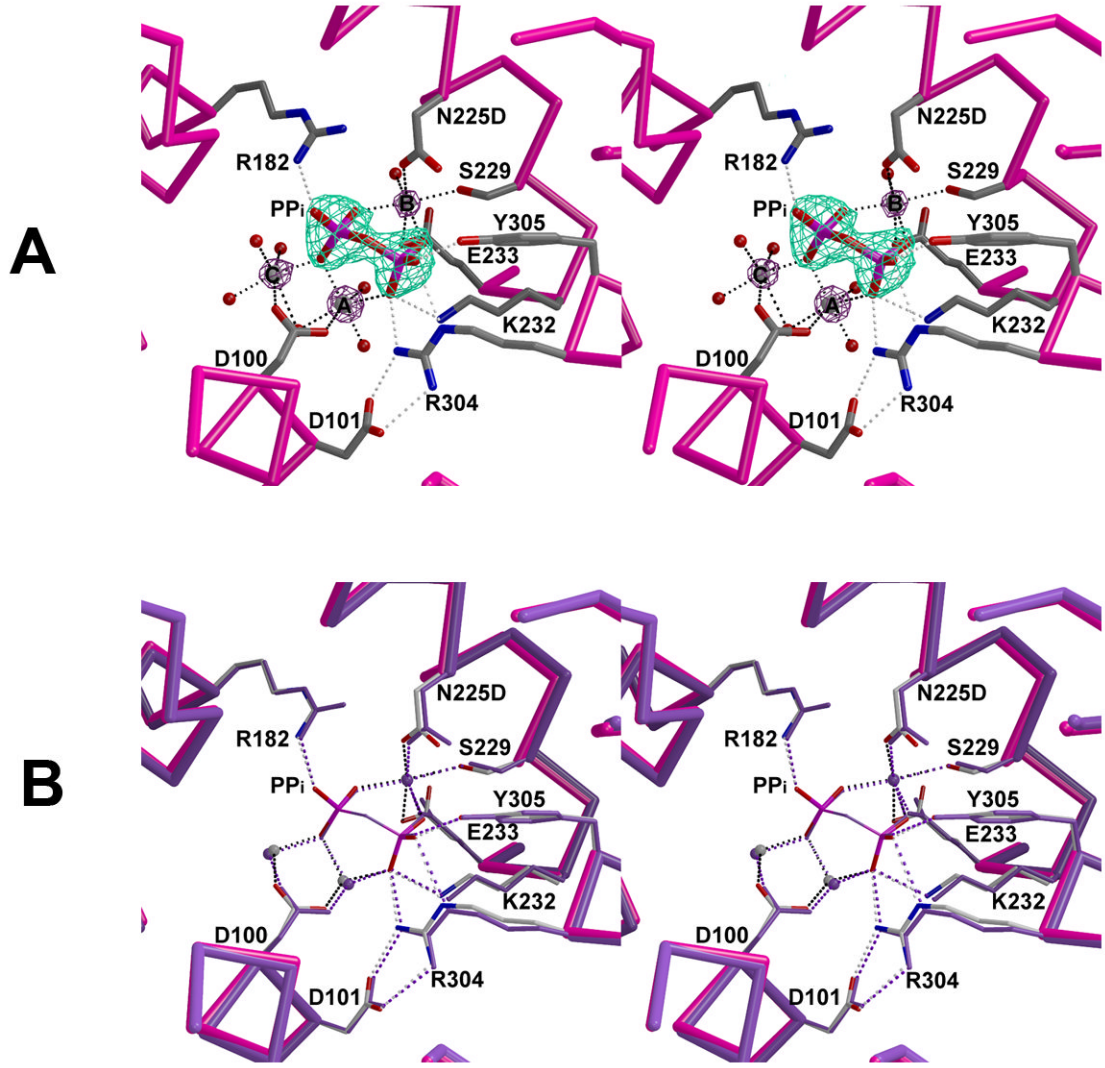

Fig. 3.

Active site of N225D trichodiene synthase complexed with Mg^{2+}_3-PP_i. **(a)** Simulated annealing omit maps of PP_i and metal ions are shown in cyan (7.5Å) and maroon (6.8σ), respectively. Metal ion coordination and hydrogen bond interactions are shown in black and gray, respectively. **(b)** Superposition of the active sites of PP_i-bound wild-type (purple) and N225D (magenta) trichodiene synthases. Note that the metal ion coordination and hydrogen bond interactions are similar in the wild-type (purple) and N225D trichodiene synthases (black and gray).

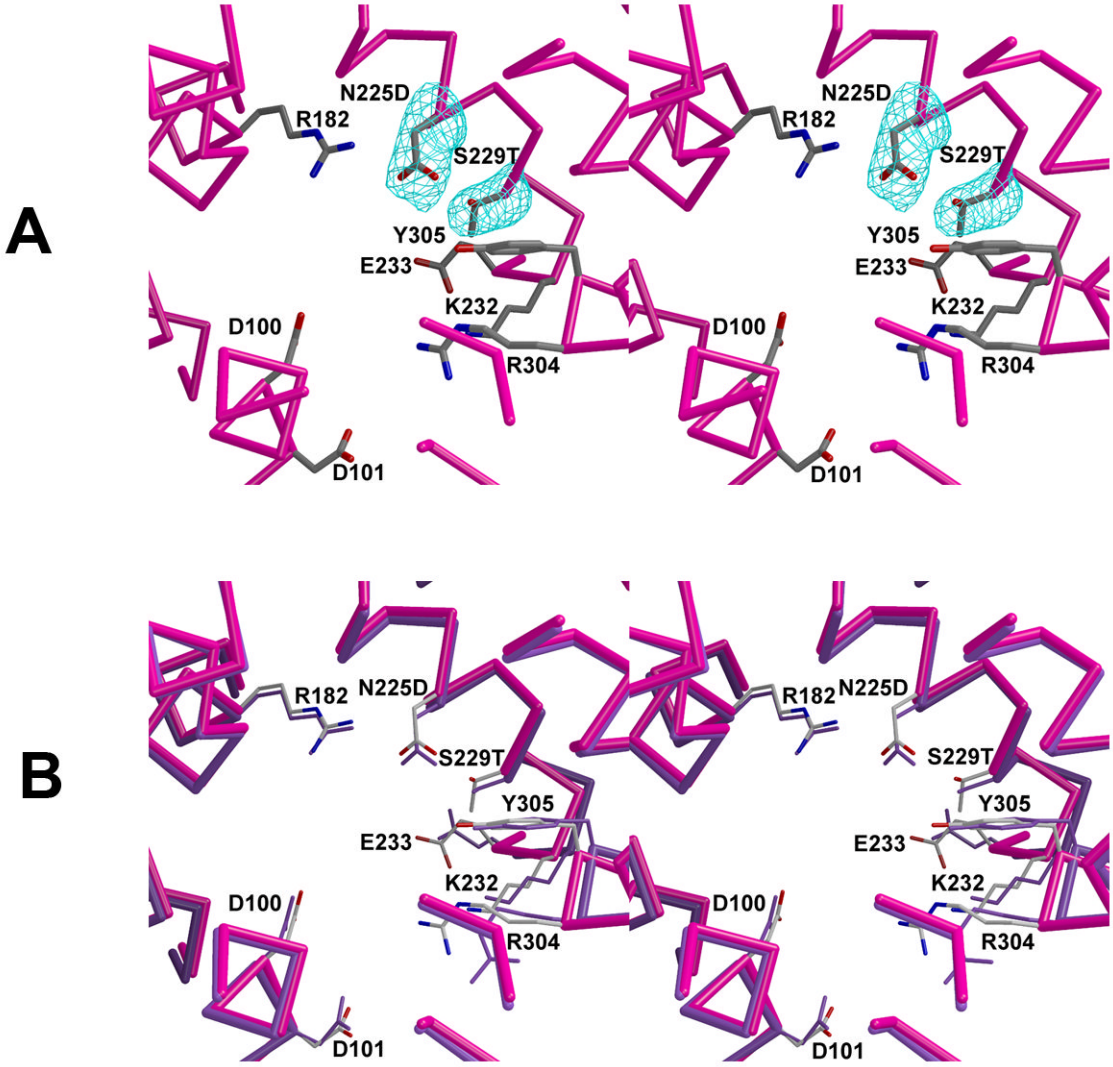

Fig. 4.

Active site of N225D/S229T trichodiene synthase. **(a)** Simulated annealing omit maps of the side chains of D225 and T229 are shown in cyan (5.0Å). **(b)** Superposition with the active site of unliganded wild-type trichodiene synthase.

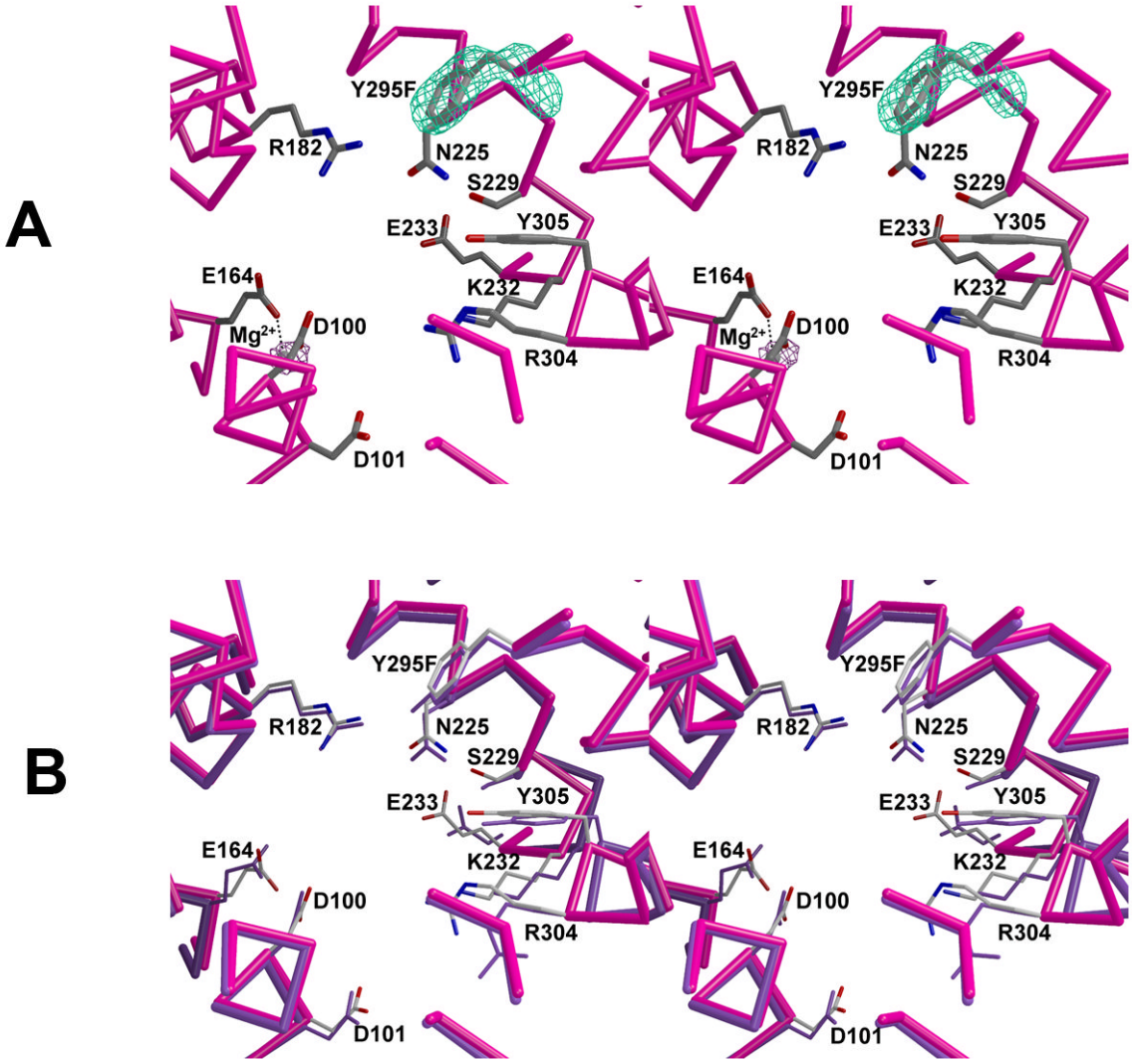

Fig. 5.

Active site of Y295F trichodiene synthase. **(a)** Simulated annealing omit maps of F295 and the Mg^{2+} ion are shown in cyan (6.0Å) and maroon (4.5Å), respectively. The Mg^{2+} ion is shown as a gray sphere. **(b)** Superposition with the active site of unliganded wild-type trichodiene synthase (purple).

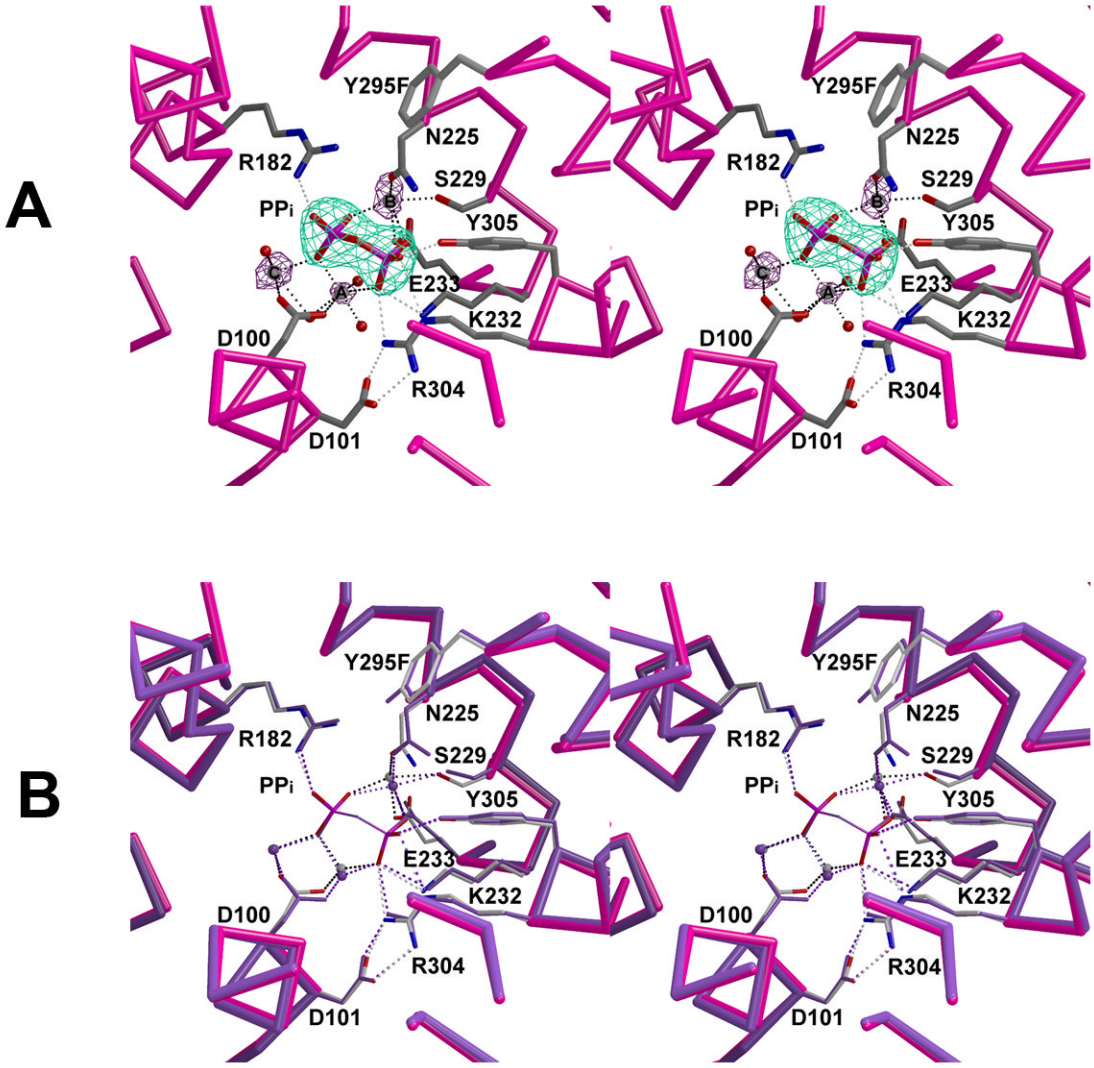

Fig. 6.

Active site of Y295F trichodiene synthase complexed with $Mg^{2+}{}_3$-PP_i. **(a)** Simulated annealing omit maps of PP_i and Mg^{2+} ions are shown in cyan (9.8Å) and maroon (7.5Å), respectively. **(b)** Superposition of the active sites of PP_i-bound wild-type (purple) and Y295F (magenta) trichodiene synthases. Note that the metal ion coordination and hydrogen bond interactions are similar in the wild-type (purple) and Y295F trichodiene synthases (black and gray).

Table I

Data Collection and Refinement Statistics

Mutant/Complex	**N225D**	**N225D-Mg^{2+}_3-PP_i**	**N225D/S229T**	**Y295F**	**Y295F-Mg^{2+}_3-PP_i**
Resolution Range (Å)	87.4-2.46	50-2.1	61.2-2.6	50-2.35	50-2.67
Reflections (measured/unique)	176908/46906	308536/76255	194477/38791	336863/54251	396431/37344
Completeness (%) (overall/outer shell)	95.9/98	99.7/100	96/90.8	98.2/97.8	100/100
R_{merge} [a] (overall/outer shell)	0.082/0.399	0.117/0.465	0.133/0.325	0.109/0.574	0.099/0.577
<I/σ> (overall/outer shell)	12.3/2.0	9.4/2.2	9.5/2.8	14.1/3.0	29.3/3.3
Protein atoms (no.)[b]	5735	5847	5750	5767	5858
Solvent atoms (no.)[b]	93	319	80	117	199
Metal ions (no.)[b]	2	3	0	2	3
Ligand atoms (no.)[b]	0	9	0	0	9
Reflections used in refinement (work/free)	44511/2338	74333/1910	36817/1940	51720/2169	35442/1867
R/R_{free} [c]	0.244/0.282	0.224/0.248	0.223/0.256	0.234/0.258	0.203/0.245
r.m.s. deviations					
bonds (Å)	0.007	0.006	0.006	0.007	0.006
angles (deg.)	1.2	1.1	1.1	1.1	1.1
dihedral angles (deg.)	18.8	18.2	18.5	18.4	18.6
improper dihedral angles (deg.)	0.8	0.7	0.8	0.7	0.8

[a] $R_{merge} = \Sigma|I_j - \langle I_j \rangle|/\Sigma I_j$, where I_j is the observed intensity for reflection j and $\langle I_j \rangle$ is the average intensity calculated for reflection j from replicate data.

[b] per asymmetric unit.

[c] $R = \Sigma||F_O| - |F_C||/\Sigma|F_O|$, where R and R_{free} are calculated by using the working and test reflection sets, respectively.

Table II

Kinetic Parameters of Mutant Trichodiene Synthases

Trichodiene synthase	k_{cat} (s^{-1})	K_M (μM)	k_{cat}/K_M ($M^{-1}s^{-1}$) (x 10^6)
Wild-type[a]	0.138 ± 0.004	0.078 ± 0.0056	1.77
N225D[b]	0.005 ± 0.0003	0.485 ± 0.016	0.01
S229T[b]	0.015 ± 0.004	6.0 ± 0.8	0.0025
N225D/S229T[b]	inactive	-	-
Y295F[b]	0.111 ± 0.005	0.069 ± 0.005	1.59

[a] From reference 26.

[b] Standard deviations for k_{cat} and K_m are the calculated statistical errors for the nonlinear least-squares regression fit of the data to the Michaelis-Menten expression, with R values typically >0.98.

Table III

Product Arrays of Wild-Type and Mutant Trichodiene Synthases[a]

	T_R[b] (min)	WT (%)[c]	D100E (%)	N225D (%)	S229T (%)	Y295F (%)
α-Barbatene	22.70	3.2	7.6	3.6	1.7	n.o.
β-Farnesene	23.81	0.5	2.5	n.o.[d]	n.o.	n.d.[e]
α-Acoradiene	24.06	n.o.	0.9	n.o.	n.o.	n.d.
β-Acoradiene	24.12	0.5	1.2	n.o.	0.5	n.d.
Isochamigrene	24.23	3.0	5.7	5.0	1.8	n.d.
α-Bisabolene	24.40	1.0	1.6	0.7	0.9	n.d.
Cuprenene	24.95	2.4	4.5	10.4	2.1	8.8
β-Bisabolene	25.12	0.9	1.4	3.1	0.9	17.5
Trichodiene	25.54	83.9	66.4	67.3	84.3	63.9
Unknown	-	4.6	8.2	9.9	7.8	9.8
(# unknown products)		(6)	(7)	(3)	(6)	(3)

[a] Estimated errors in the percentages listed is generally less than 5% for major products but can range as high as 10–20% for minor products due to possible errors associated with baseline estimation in gas chromatograms.

[b] T_R: Retention time in *n*-pentane, using GC/MS (CI); T_R for unknown products range from 22.80 to 26.00 min.

[c] WT: Wild-type trichodiene synthase.

[d] n. o.: Not observed under experimental conditions.

[e] n. d.: Ratio not determined due to low concentration of product.